Hyperfine Interact
DOI 10.1007/s10751-014-1045-4

Structure and occurrences of ≪ green rust ≫ related new minerals of the ≪ *fougérite* ≫ group, *trébeurdenite* and *mössbauerite*, belonging to the ≪ hydrotalcite ≫ supergroup; how Mössbauer spectroscopy helps XRD.

J.-M. R. Génin · A. Christy · E. Kuzmann · S. Mills · C. Ruby

Abstract Mössbauer spectroscopy yields decisive information for interpreting x-ray diffraction (XRD) patterns in the case of 'green rusts" with intercalated CO_3^{2-} anions, i.e. the chemical analogs of the three minerals that constitute within the ≪ hydrotalcite ≫ supergroup comprising 44 minerals the "*fougèrite*" group where the structure stays globally unchanged. The only difference comes from the deprotonation of OH^- ions at the apices of the octahedrons occupied by the Fe cations so that Fe^{II} ions become Fe^{III}. Low angle x-ray diffraction using synchrotron radiation displays the presence of many polytypes which reflects the stacking of brucite like layers and anion interlayers so that a 2D long range order of anions stays unchanged from *fougèrite* to *mössbauerite*.

Keywords $Fe^{II–III}$(oxy)hydroxycarbonate · Green rust · Mössbauer spectroscopy · *Fougèrite* · *Trébeurdenite* · *Mössbauerite* · Polytypes

Proceedings of the 32nd International Conference on the Applications of the Mössbauer Effect (ICAME 2013) held in Opatija, Croatia, 1–6 September 2013

J.-M. R. Génin (✉) · C. Ruby
Institut Jean Barriol, ESSTIN-Université de Lorraine, 2 rue Jean Lamour, 54500 Vandœuvre-lès-Nancy, France
e-mail: jean-marie.genin@univ-lorraine.fr

A. Christy
Centre for Advanced Microscopy, Australian National University, Sullivans Creek Road, Canberra 0200, ACT, Australia

E. Kuzmann
Department of Chemistry, Eötvös Lorand University, Pazmany Peter setany, 1117 Budapest, Hungary

S. Mills
Geosciences, Museum Victoria, GPO Box 666, Melbourne 3001, Victoria, Australia

Published online: 11 April 2014

1 Introduction

The discovery of the minerals that are responsible for the bluish-green colour of gleysols in continental aquifers and maritime marshes is, by many aspects, of utmost importance because of their ubiquity over the earth; they play a major role in the purification of water in natural conditions due their outstanding redox properties [1–3]. As part of the "hydrotalcite supergroup" [4], they are closely related to the Fe^{II-III} hydroxycarbonate green rust, $GR(CO_3^{2-})$, which was originally studied for its intermediate role during the corrosion of iron-based materials [5–7].

$GR(CO_3^{2-})$ that belongs to the layered double hydroxide (LDH) family consists in stacking brucite-like $[Fe^{II}_4Fe^{III}_2(OH)_{12}]^{2+}$ layers that alternate with $[CO_3 \cdot 3\ H_2O]^{2-}$ interlayers within R-3m space group [8, 9]. It usually gets oxidized into ferrihydrite that evolves to goethite by aerial oxidation as observed during the corrosion process of steels [5, 6, 10, 11]. However, another process occurs if the dissolution of the compound is not allowed by *in situ* oxidation into so called "ferric green rust" $GR(CO_3^{2-})$*, $[Fe^{III}_6O_{12}H_8]^{2+}\cdot[CO_3\cdot 3\ H_2O]^{2-}$, where some OH^- ions get deprotonated [12, 13]. In this paper, we show that the crystallographic structure of the compounds related to the minerals is now fully understood by using x-ray diffraction (XRD) completed by successive Mössbauer studies. But it is in fact Mössbauer spectroscopy, which is at the origin of the discovery of the three minerals, *fougèrite*, *trébeurdenite* and *mössbauerite* [14–17], even though their existence has been definitively confirmed since by XRD.

2 Ordering of Fe cations and anions in "green rusts"

XRD gives first information concerning the stacking of layers and interlayers in green rusts: "green rust one" for those that incorporate spherical or planar anions such as Cl^-, CO_3^{2-}, $C_2O_4^{2-}$ and $HCOO^-$ or "green rust two" for those that incorporate tetrahedral anions such as SO_4^{2-} and SeO_4^{2-}. The stacking sequence for OH^- sublayers in the first case can be designated as *A, B, B, C, C, A*... where *A*, *B* and *C* are the three sites in the hexagonal pavement. Mössbauer spectra measured at 78 K display three quadrupole doublets D_1, D_2 and D_3, where D_1 and D_2 with a large quadrupole splitting are attributed to two different ferrous sites and D_3 with a small splitting is attributed to ferric ions (Fig. 1). All these sites have been interpreted the same way for all types of anion in all "green rusts one". D_1 corresponds to Fe^{2+} ions which have no influence from the anion whereas D_2 corresponds to Fe^{2+} ions which are in register to an anion. The relative abundances of the three doublets characterize which anion one deals with depending on its size, shape and charge (Table 1).

Firstly, the ferric ionic ratio $x = \{[Fe^{3+}] / ([Fe^{2+}] + [Fe^{3+}])\}$ is directly evaluated by the relative abundance of D_3. One observes that all experimental values lie in the range [1/4, 1/3] (Table 1) [6, 18–23]. This reflects a 2D long range order of the Fe^{3+} cations due to electrostatic repulsion; therefore, each Fe^{3+} ion is surrounded by six Fe^{2+} ions in the hexagonal cation sublayer. There exist three possibilities: (i) order α where the periodicity is $(2\times\boldsymbol{a})$ with $x = 1/4$, (ii) order β where the periodicity is $(\sqrt{3}\times\boldsymbol{a})$ with $x = 1/3$ and (iii) order γ where the periodicity is $(7\times\boldsymbol{a})$ with $x = 2/7$ if the parameter of the hexagonal pavement is called $\boldsymbol{a}$. The three cases are observed (Table 1).

The value of x depends on the concerned anion. A 2D long range order of anions in sublayers can explain these values as due to the charge, size and shape of the considered anion. This 2D order of anions must be consistent with that of the Fe^{3+} cations since the

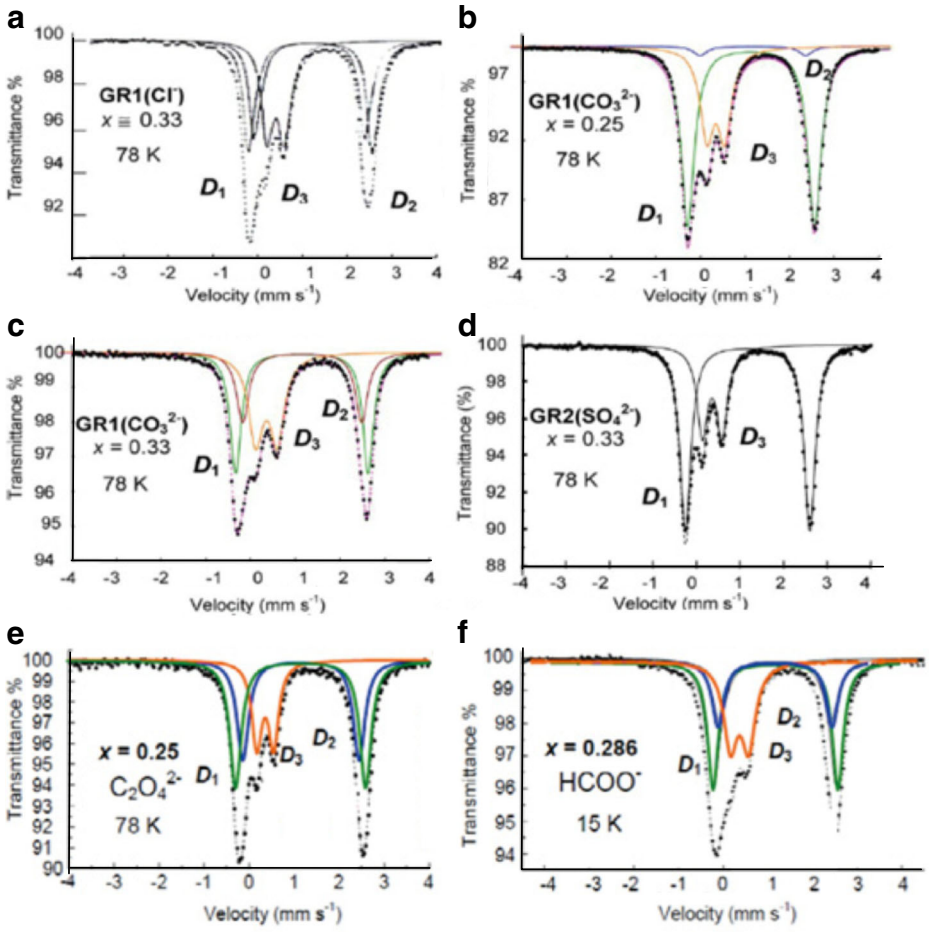

Fig. 1 Mössbauer spectra measured at 78 K of various *green rusts*: **a** GR1(Cl^-) at $x = 0.33$, **b** GR1(CO_3^{2-}) at $x = 0.25$, **c** GR1(CO_3^{2-}) at $x = 0.33$, **d** GR2(SO_4^{2-}) at $x = 0.33$, **e** GR1($C_2O_4^{2-}$) at $x = 0.25$, **f** GR1($HCOO^-$) at $x = 0.285$

meshes must match. Moreover, the D_1 and D_2 relative abundances allow us to check the validity of the corresponding order for the Fe^{3+} cations as drawn in Fig. 2.

Let us consider the case when carbonate anions constitute the interlayers with water molecules. Values of x are 0.25 or 0.33 and corresponding formulae are $Fe^{II}_6Fe^{III}_2(OH)_{16}CO_3{\cdot}5H_2O$ or $Fe^{II}_4Fe^{III}_2(OH)_{12}CO_3{\cdot}3H_2O$ for the Fe^{II-III} oxyhydroxicarbonate, respectively. Intermediate values of x can be obtained but they are in fact a mixture of topotactic domains with $x = 0.25$ and 0.33. For $x = 0.33$, the periodicity of Fe^{3+} ions in the cation sublayers is ($\sqrt{3}\times \boldsymbol{a}$) (Fig. 3a) and the matching 2D order in the carbonate interlayers has a periodicity of ($2\sqrt{3}\times \boldsymbol{a}$) (Fig. 3b). This comes from the two configurations that CO_3^{2-} anions may take, Δ or ∇. Assuming for instance that Fe^{2+} ions of Fig. 3a are in an *A* site (we shall call it later α for Fe cations), the O^{2-} ions within a carbonate anion is at a *B* site (later called *b*); the center of the carbonate is in an *a* or a *c* position whether one deals with the ∇ or Δ configuration. Consequently, one Fe^{2+} ion is in register to the center of a

Table 1 Hyperfine parameters of Mössbauer spectra of GRs measured at 78 K as illustrated in Fig. 1 and selected from the literature

x	GR1 (Cl^-) 0.25 at 78 K			GR1 (Cl^-) 0.33 at 78 K			GR1 (CO_3^{2-}) 0.25 at 78 K			GR1 (CO_3^{2-}) 0.33 at 78 K			GR1 (SO_4^{2-}) 0.33 at 78 K			GR1 ($C_2O_4^{2-}$) 0.25 at 78 K			GR1 ($HCOO^-$) 0.286 at 15 K		
	δ mm s^{-1}	Δ	RA %	δ mm s^{-1}	Δ	RA %	δ mm s^{-1}	Δ	RA%	δ mm s^{-1}	Δ	RA %	δ mm s^{-1}	Δ	RA %	δ (mm s^{-1})	Δ	RA %	δ (mm s^{-1})	Δ	RA %
D_1	1.26	2.88	48	1.27	2.89	37	1.28	2.97	62	1.27	2.93	51	1.27	2.88	66	1.28	2.84	42.7	1.28	2.75	47 ± 4
D_2	1.25	2.60	24	1.25	2.60	32	1.28	2.55	12	1.28	2.64	15				1.28	2.58	31.7	1.28	2.48	24.5 ± 4
D_3	0.47	0.41	24	0.47	0.41	31	0.47	0.43	26	0.47	0.42	34	0.47	0.44	34	0.48	0.37	25.6	0.48	0.37	28.5 ± 1

x Observed values of x that depend on the charge, size and shape of the anion

1/4	$C_2O_4^{2-}$		F^-	Cl^-	I^-	CO_3^{2-}	
2/7		$HCOO^-$					
1/3			F^-	Cl^-	I^-	CO_3^{2-}	SO_4^{2-}	SeO_4^{2-}

δ(mm s^{-1}); isomer shift (α-iron as reference at ambient), Δ (mm s^{-1}): quadrupole splitting, *RA* (%): relative abundance

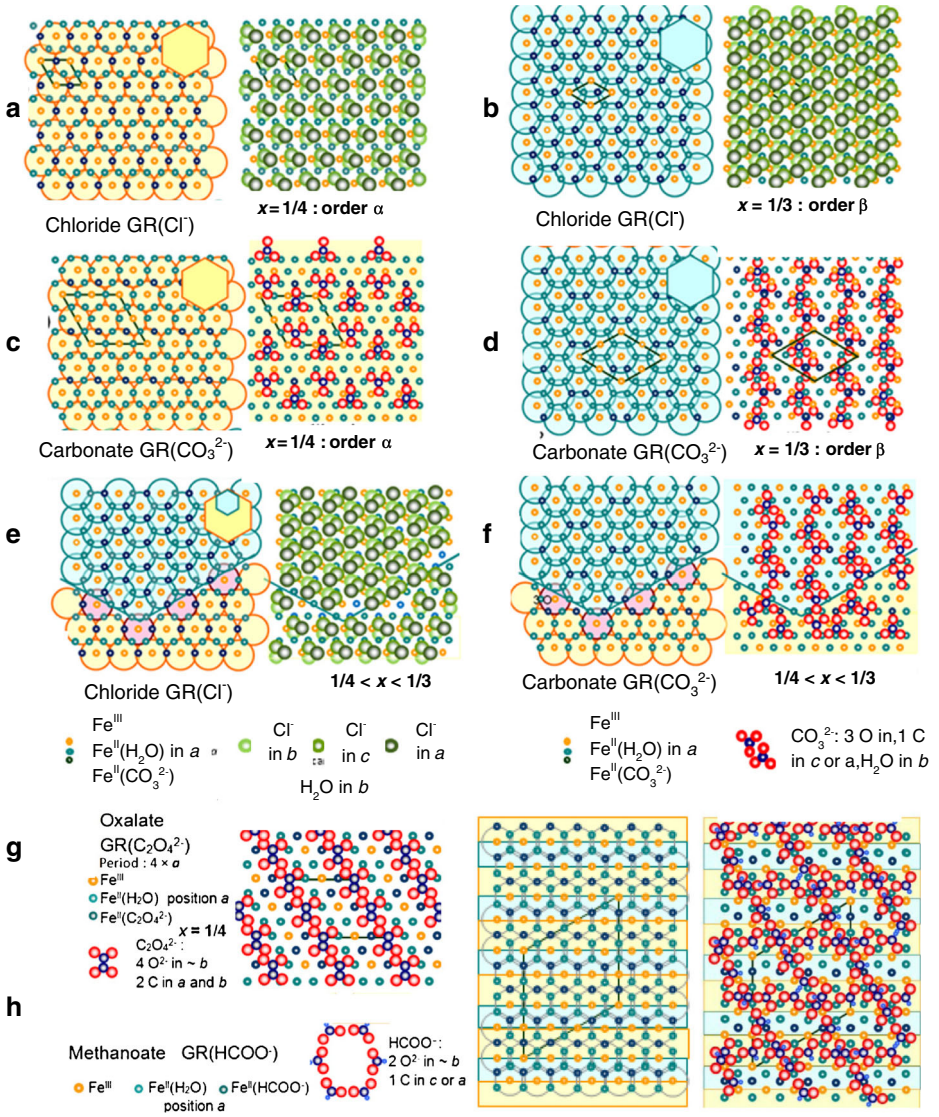

Fig. 2 (001) projections perpendicular to the ***c*** axis of the rhomboedral lattice of GR1 for Fe cation layers (*left*) and corresponding anion interlayers (*right*) displaying long range order types in the case of **a** Fe^{II-III} hydroxychloride GR1(Cl^-) with order α at $x = 1/4$ and periodicity $4 \times \boldsymbol{a}$. A third interlayer is displayed to designate $Fe^{II}(Cl^-)$; **b** GR1(Cl^-) with order β at $x = 1/3$ with periodicity $2\sqrt{3} \times \boldsymbol{a}$. A third interlayer is displayed to designate $Fe^{II}(Cl^-)$; **c** any intermediate composition for GR1(Cl^-) is constituted of a mixture of domains with 3-fold symmetry of types α and β. A third interlayer is displayed to designate $Fe^{II}(Cl^-)$; **d** Fe^{II-III} hydroxycarbonate GR1(CO_3^{2-}) with order α at $x = 1/4$ and periodicity $4 \times \boldsymbol{a}$; **e** GR1(CO_3^{2-}) with order β at $x = 1/3$ with periodicity $2\sqrt{3} \times \boldsymbol{a}$; **f** any intermediate composition for GR1(CO_3^{2-}) is constituted of a mixture of domains with 3-fold symmetry of types α and β; **g** GR1 ($C_2O_4^-$) with order α at $x = 1/4$ with periodicity $2\sqrt{3} \times \boldsymbol{a}$ and **h** GR1($HCOO^-$) with order γ at $x = 2/7$ with periodicity $7 \times \boldsymbol{a}$

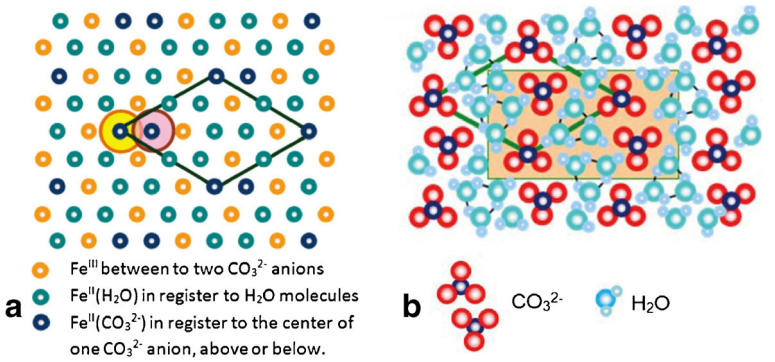

Fig. 3 Projection perpendicular to the ***c*** axis: **a** Fe cations sublayer in GR(CO_3^{2-}) ($x = 1/3$) showing three Fe environments : Fe^{3+} ions between two CO_3^{2-} ions, one above and one below, Fe^{2+} ions in register to water molecules above and below, Fe^{2+} ions in register to the center of one CO_3^{2-} anion, above or below; **b** the 2D long range order of CO_3^{2-} anions in interlayers and its rhombic mesh that matches the 2D order in Fe sublayers

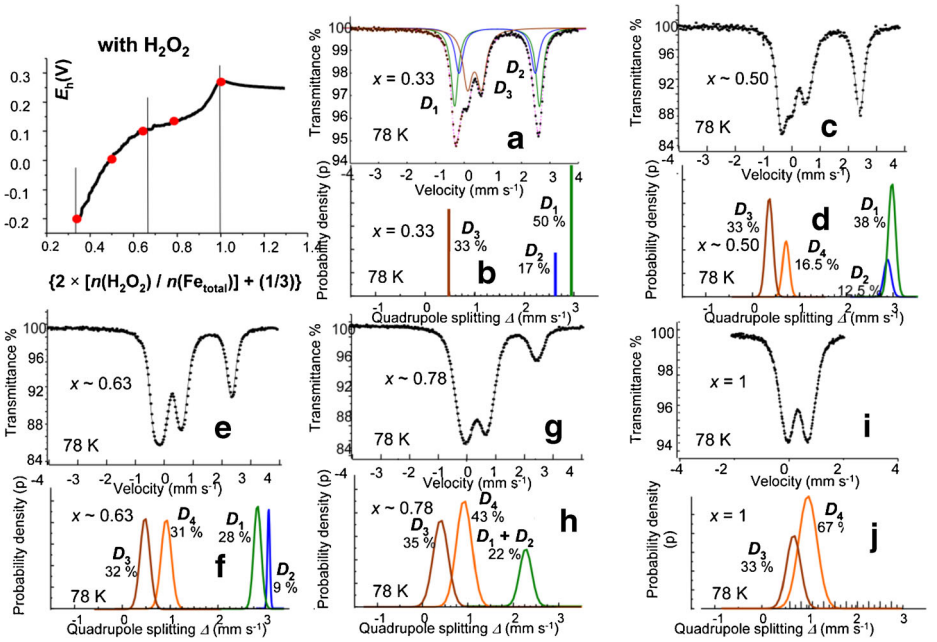

Fig. 4 Mössbauer spectra measured at 78 K of synthetic "*green rust*" samples for values of $x = [Fe^{3+}]/[Fe_{total}]$ in the range [1/3,1]. *Top right*: Electrode potential E_h versus x during the *in situ* deprotonation. **a** Total spectrum showing fitted doublets for $x = 1/3$ and **b** Probability density for Gaussian distributions of quadrupole splittings fitted using Voigt-function profiles; **c** and **d** are corresponding data for $x = 1/2$; **e** and **f** for $x = 0.63$; **g** and **h** for $x = 0.78$; **i** and **j** for $x = 1$

carbonate of the interlayer lying above the sublayer and another Fe^{2+} ion is in register to the center of a carbonate of the interlayer lying below. The overall periodicity is governed by the periodicity of the anions in interlayers; back to Fig. 3a, one sees that within a 2D unit cell, there are among twelve cations, four Fe^{3+} ions, six Fe^{2+} ions in register to water molecules and two Fe^{2+} ions in register to the center of two CO_3^{2-} anions, one above and one below. The D_1: D_2: D_3 abundance ratios of 1/2: 1/6: 1/3 is thus properly explained (Fig. 1c, Table 1).

3 *In situ* deprotonation of carbonated green rusts

The *in situ* deprotonation of carbonated green rust has been already fully reported [11–13]. A synthetic GR(CO_3^{2-}) was prepared by coprecipitation at $x = 1/3$. Then, hydrogen peroxide is gradually introduced in the beaker with a peristaltic pump whereas the electrode potential E_h increased continuously in contrast to the usual oxidation process where the green rust dissolves before precipitating a ferric oxyhydroxide [10, 11] (Fig. 4). Meanwhile the color of the solution in the beaker went from bluish-green to orange through olive green. Five samples were dried under nitrogen atmosphere and measured by Mössbauer spectroscopy. Values of x were evaluated since they corresponded to $\{2 \times [n(H_2O_2) / n(Fe_{total})] + 1/3\}$. The evolution of the spectra showed that the intensity of the ferrous quadrupole doublets D_1 and D_2 decreased while a new ferric doublet D_4 appeared (Fig. 4a-j). Clearly the Fe^{2+} ions got oxidized into Fe^{3+} ions. The process occurred by deprotonation of OH^- ions at the apices of the octahedron that surrounded each Fe cation. Doublet D_4 corresponds to the Fe^{3+} ions due to deprotonation in contrast to the previous Fe^{3+} ions corresponding to D_3, the relative abundance of which remained at 1/3. The fitting procedure was the use of mere Lorentzian lines for the starting GR at $x = 1/3$. The four other spectra for $x = 0.50$, 0.63, 0.78 and 1 needed to use a deconvolution of Gaussian distributions and Lorentzian-shape lines (Table 2). If the relative abundance of D_3 stayed constant at 1/3, those of D_1 and D_2 remained in the 3: 1 ratio while decreasing when x increased (Fig. 5). Finally, the ferric GR(CO_3^{2-})*, which is in fact brownish orange, displayed two ferric doublets D_3 and D_4 in the 1: 2 abundance ratio.

The evolution of the corresponding XRD patterns was followed (Fig. 6). All lines that characterized the 3^- space group were still present even though their position shifted slightly towards higher angles while they decreased and broadened. This was attributed to a small contraction of the lattice parameter in the hexagonal plane while the octahedral site got distorted since some OH^- ions became O^{2-} ions. Transmission electron micrographs (not represented) displayed the same hexagonal platelets whatever the value of x even though the apices got blurred in particular for the ferric GR*. All these features could make us think that we were dealing with a solid solution with a continuous value of x and the formula $Fe^{II}_{(1-6x)}Fe^{III}_6xO_12H_{2(7-3_x)}$ $CO_3 \cdot 3$ H_2O was forwarded. Voltammetric cycling showed also that the same phenomenon could occur by protonation of OH^- ions allowing to obtain a completely ferrous compound at $x = 0$ [13, 24]. Therefore x seemed to vary in the complete [0-1] range. The average formula which is measured by Mössbauer spectroscopy $Fe^{II}_{6(1-x)}Fe^{III}_{6x}O_{12}H_{2(7-3)}$ $CO_3 \cdot 3H_2O$ is in fact obtained by mixing these ordered compounds.

However, only OH^- ions became O^{2-} ions during deprotonation or only OH^- ions became H_2O molecules during protonation. Projections of layers are displayed in Fig. 7. One notes that starting from GR(CO_3^{2-}) at $x = 1/3$, in the first case, O^{2-} ions induced that

Table 2 Mössbauer parameters for "green rusts" with $x = [Fe^{3+}]/[Fe_{total}] \in [1/3, 1]$ when adding H_2O_2 to $GR(CO_3^{2-})$

	Quadrupole doublets	δ (mm s^{-1})	$< \Delta >$ (mm s^{-1})	$< \sigma\Delta >$ (mm s^{-1})	RA (%)	F (%)	T (%)	M (%)
$x = 0.33$						100		
Fe^{2+}	D_{1f}	1.25	2.92	0	50			
	D_{2f}	1.25	2.63	0	17			
Fe^{3+}	D_{3f}	0.48	0.47	0	33			
$x \sim 0.50$						50	50	
Fe^{2+}	$D_{1f} + D_{1t}$	1.21	2.98	0.14	38			
	$D_{2f} + D_{2t}$	1.21	2.72	0.16	12.5			
Fe^{3+}	$D_{3f} + D_{3t}$	0.49	0.40	0.15	33			
	D_{4t}	0.49	0.70	0.28	16.5			
$x \sim 0.63$						9	91	
Fe^{2+}	D_{1t}	1.24	2.80	0.15	28			
	D_{2t}	1.24	3.05	0.05	9			
Fe^{3+}	D_{3t}	0.48	0.49	0.20	32			
	D_{4t}	0.48	0.90	0.21	31			
$x \sim 0.78$							66	34
Fe^{2+}	$D_{1t} + D_{2t}$	1.21	2.89	0.31	22			
Fe^{3+}	$D_{3t} + D_{3m}$	0.47	0.45	0.32	35			
	$D_{4t} + D_{4m}$	0.47	0.95	0.34	43			
$x = 1$								100
Fe^{3+}	D_{3m}	0.47	0.60	0.30	33			
	D_{4m}	0.47	0.88	0.41	67			

δ: isomer shift (α-iron as reference at ambient), Δ: quadrupole splitting; $< \sigma\Delta >$: standard deviation of quadrupole splitting; RA: relative abundance; F: fougèrite; T: trébeurdenite; M: mössbauerite

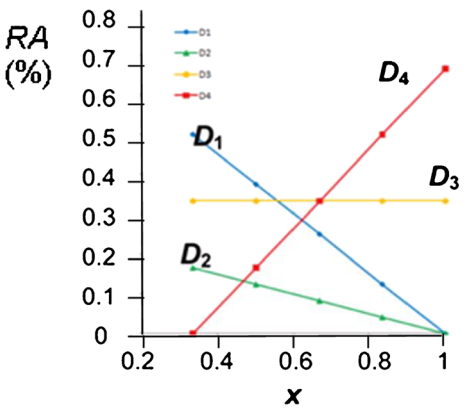

Fig. 5 (*Left*) Relative abundance of Fe cation environments measured (Table 2) from quadrupole doublets D_1–D_4 versus x

Fe^{2+} became Fe^{3+} and, in the second case, H_2O molecules induced that Fe^{3+} became Fe^{2+}. Neither Fe cations nor carbonate anions moved. Moreover, the study by Mössbauer spectroscopy of the magnetic properties of the deprotonation process, which is out of the scope

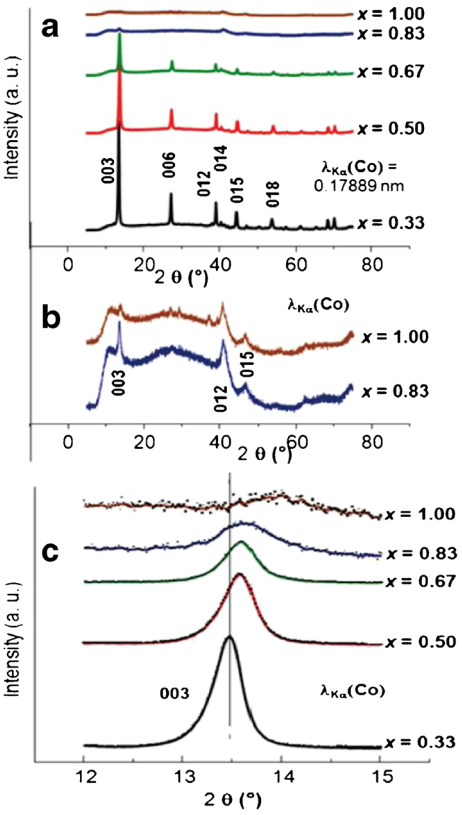

Fig. 6 (*Right*) XRD patterns of "*green rust*" samples during deprotonation, for $x = [Fe^{3+}]/[Fe_{total}]$ ranging from [1/3, 1]. **a** all patterns using the same scale for intensity, **b** details for $x = 0.83$ and 1, **c** the (003) lines only, proving the contraction of the lattice with x and broadening as a result of strain from progressive deprotonation

of this paper, showed that definite ordered phases displaying specific and distinct behavior exist [15, 25, 26]:

(i) at $x = 1/3$, i.e. GR(CO_3^{2-}) with formula $Fe^{II}_4Fe^{III}_2(OH)_{12}CO_3{\cdot}3H_2O$, the Fe^{II-III} hydroxycarbonate is ferrimagnetic; all Fe^{3+} ions are surrounded by six Fe^{2+} ions and the two sublattices, ferric and ferrous, are antiparallelly coupled; the Néel temperature is 5 K (Fig. 7b).

(ii) at $x = 2/3$, i.e. $Fe^{II}_2Fe^{III}_4O_{12}H_{10}CO_3{\cdot}3\ H_2O$, the Fe^{II-III} oxyhydroxycarbonate is also ferrimagnetic; all Fe^{2+} ions are surrounded by six Fe^{3+} ions and the two sublattices, ferric and ferrous are also antiparallelly coupled; the Néel temperature is now about 30 K (Fig. 7d);

(iii) at $x = 1$, the ferric oxyhydroxycarbonate GR(CO_3^{2-})*, $Fe^{III}_6O_{12}H_8\ CO_3{\cdot}3H_2O$ is ferromagnetic; the Curie temperature is around 80 K with a strong superparamagnetic behavior (Fig. 7f).

For reasons we shall see later, the three ordered compounds at $x = 1/3$, 2/3 and 1 are now called, *fougèrite* ***F***, *trébeurdenite* ***T*** and *mössbauerite* ***M***, respectively. The average formula obtained by mixing these compounds, i.e. $Fe^{II}_{6(1-x)}Fe^{III}_{6x}O_{12}H_{2(7-3x)}\ CO_3{\cdot}3H_2O$, is in the range [1/3, 2/3] a mixture of ***F*** and ***T*** and their proportions are obtained by the lever rule: $[(2-3x)\boldsymbol{F} + (3x\text{-}1)\boldsymbol{T}]$ (Fig. 7c), whereas, in the range [2/3, 1], it is a mixture of ***T*** and ***M*** with proportions $[3(1\text{-}x)\boldsymbol{T} + (3x\text{-}2)\boldsymbol{M}]$ (Fig. 7e). During the *in situ* deprotonation process, the more oxidized phase grows topotactically, e.g. ***T*** at the expense of ***F*** (Fig. 7c) or ***M*** at the

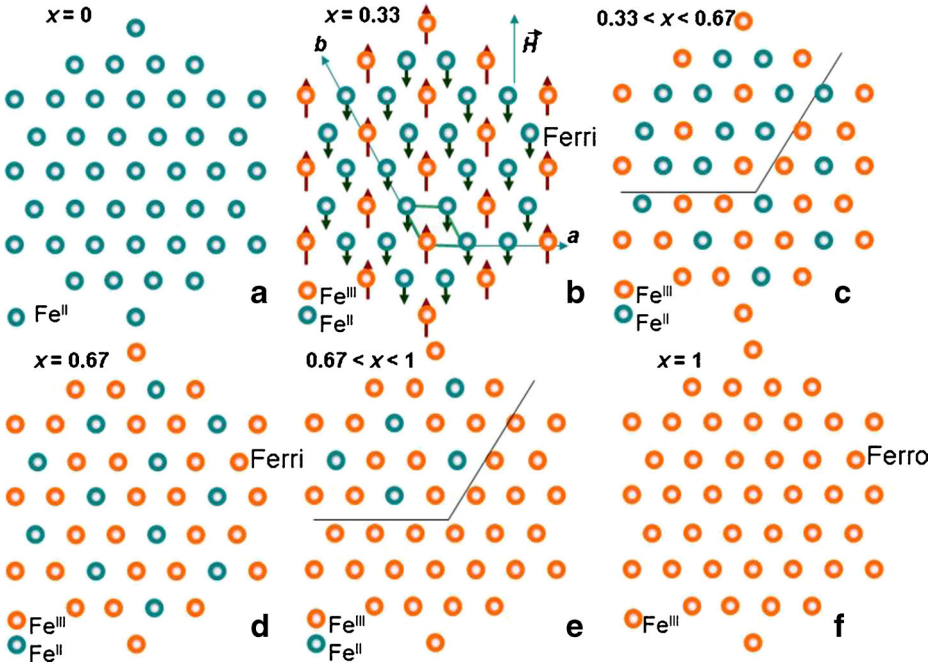

Fig. 7 Ordering of $Fe^{2+}$and Fe^{3+} cations within the octahedral sublayer leading to various magnetic properties: **a** $Fe_6^{2+}(OH)_{10}(H_2O)_2CO_3{\cdot}.3H_2O$; **b** $Fe_4^{2+}Fe_2^{3+}(OH)_{12}CO_3.3H_2O$, showing spin coupling of Fe^{2+} and Fe^{3+} ions; **c** $Fe_2^{2+}Fe_4^{3+}O_2(OH)_{10}CO_3{\cdot}.\ 3H_2O$; **d** $Fe_6^{3+}O_4(OH)_8CO_3.3H_2O$

expense of ***T*** (Fig. 7e). Because of experimental difficulties, no information is known yet about the properties of the ferrous compound ***A***, but it is reasonable to extend the topotactical reaction over the whole [0–1] range.

The various Fe sites that are distinguished by Mössbauer data (Table 2) correspond to the four quadrupole doublets as also represented in Fig. 8a–c. A three-dimensional representation of the structure is drawn in Fig. 9a–c if the 3^- space group is respected. There is a 120° rotation from one layer to the next one. Thus, the periodicity ***c*** perpendicularly to the layers comprises three layers and three interlayers. Lattice parameters as measured from XRD data are gathered in Table 3. Values of x experimentally obtained are approximately 0.50, 0.63 and 0.78 and precisely 0.33 and 1. Spectra are measured at 78 K (Fig. 4) and fitted using a Voigt profile. δ : isomer shift in mm s^{-1} (reference is α-iron at ambient), $< \Delta >$: mean value of quadrupole splitting in mm s^{-1} and $< \sigma\Delta >$: its standard deviation; *RA* (%): relative area of peak doublets as a percentage of total intensity."*F* (%)", "*T* (%)" and "*M* (%)" indicate respectively the molar percentages of *fougèrite*, *trébeurdenite* and *mössbauerite* in the mixture, deduced from bulk composition according to the lever rule.

4 Polytypes

4.1 Experimental

Small angle diffraction experiment was recently performed at the Zürich synchrotron facility using ferric $GR(CO_3^{2-})$* samples; no special care against oxidation was needed. The

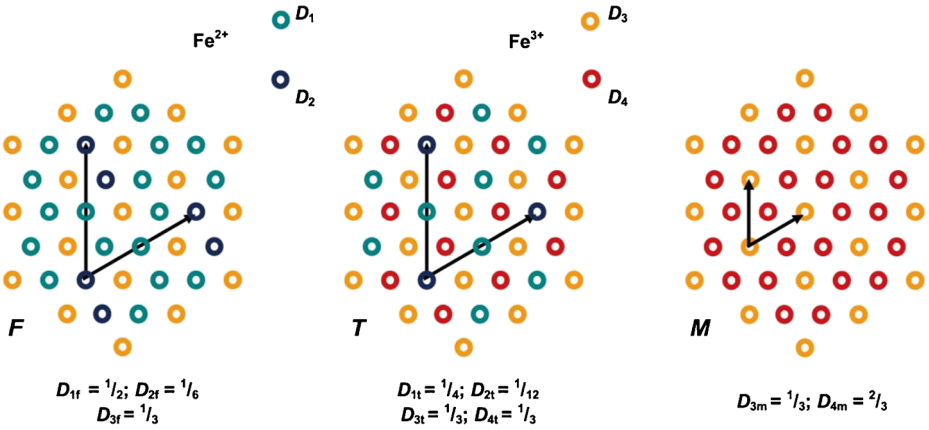

Fig. 8 Cations in octahedral sublayer of *fougèrite* (***F***), *trébeurdenite* (***T***) and *mössbauerite* (***M***), showing two-dimensional superstructures that arise when Fe^{2+} and Fe^{3+} cations get ordered as in Fig. 7 and D_2 and D_3 environments which are clustered near interlayer carbonate. *Arrows* indicate translation vectors between equivalent Fe sites

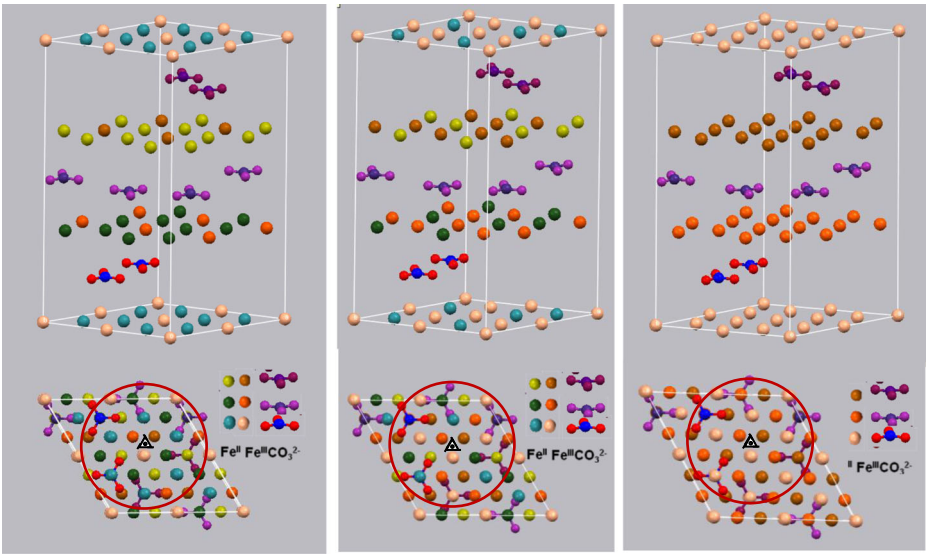

Fig. 9 **a** *Fougèrite*, $Fe^{II}_4Fe^{III}_2(OH)_{12}CO_3 \cdot 3H_2O$, **b** *trébeurdenite* $Fe^{II}_2Fe^{III}_4O_2(OH)_{10}CO_3 \cdot 3H_2O$, and **c** *mössbauerite* $Fe^{III}_6O_4(OH)_8CO_3 3H_2O$ unit cells for the "perfect" crystal, i.e. $3R_1$ polytype; OH^- and H_2O are not represented

Table 3 Interplanar distances d_{hkl} and cell parameters of R-3m space group GR(CO_3^{2-})* computed from XRD patterns and data versus ferric fraction $x = \{[Fe^{III}]/[Fe_{total}]\}$ (Fig. 6)

x	0.33	0.50	0.67	0.83	1
d_{003} (Å)	7.632	7.569	7.565	7.54	~7.34
d_{012} (Å)	2.679	2.669	2.672		
$\boldsymbol{c}$ (Å)	22.896	22.707	22.695		
$\boldsymbol{a}$ (Å)	3.182	3.169	3.173		

finely crushed powder was introduced in a 1 mm glass capillary and was checked with a standard powder X-ray diffraction device using a Mo Kα_1 radiation. Then, the high resolution pattern was performed by using a monochromatic wavelength set at $\lambda = 0.350156$ Å with the synchrotron. Patterns were recorded in continuous scanning mode in the 2θ range between 0°and 52° during two hours (Fig. 11 in yellow). The wavelength was selected with a double-crystal Si (111) monochromator, calibrated and refined using Si NIST powder ($\boldsymbol{a} = 5.43094$ Å) from the position of the first ten Si reflections. Then, the pattern was transliterated to the more familiar Mo Kα_1 radiation with a 0.7093 Å wavelength (Fig. 11 in blue). Three sets of peaks were detected: one at 7.4 Å attributed to (003) line, another one at a lower angle of 22.2 Å (3×7.4 Å) and a last one in the way between at 14.06 Å. These two sets of peaks are interpreted in connection with the polytypes existing in the GR(CO_3^{2-})* crystals.

4.2 Models

The structural model we presented previously for the "perfect crystal" (Fig. 9) i.e. the $3R_1$ polytype of the recent nomenclature [4], displayed the 2D Fe cation order in sublayers at the origin of the 2D CO_3^{2-} anion order within the adjacent interlayers. The question of anions ordering within interlayers was obliterated up till now in this general nomenclature, since the information provided by XRD patterns did not present any proof of a 3D superlattice of anions. However, the existence of the ferric ordering in sublayers for GR(CO_3^{2-}) at $x = 1/3$ was discussed as a consequence of the Mössbauer spectra (Fig. 1c). Here we intend to show that these spectra can only be consistent with a 2D order of CO_3^{2-} anions in interlayers and that consequently the overall interaction between layers and interlayers is strictly limited to the layers above and below an interlayer and vice versa. No direct coupling among Fe sublayers or interlayers in a longer range along the $\boldsymbol{c}$ axis exists.

Information obtained from Mössbauer spectra is relative to hyperfine interactions, i.e. the immediate environment of each Fe nucleus; the quadrupole doublets relate to the influence of the charges of the six first nearest Fe neighbors within a sublayer: six OH^- ions at the apices of the surrounding octahedron and species in register to the Fe^{57} probe within the two interlayers that lie above and below, i.e. H_2O or CO_3^{2-} for D_1 or D_2, respectively. A 2D unit cell that contains two CO_3^{2-} anions corresponding to a ($2\sqrt{3} \times \boldsymbol{a}$) periodicity in an interlayer matches four adjacent meshes in each Fe sublayer, one above and one below, with periodicity ($\sqrt{3} \times \boldsymbol{a}$) (Fig. 3). Since the CO_3^{2-} ions display two possible configurations Δ and ∇ for getting the same environment from above and below, the matching mesh in the Fe sublayers comprises 12 Fe cations with 4 Fe^{3+} ions ($x = 1/3$) (Fig. 3). If the oxygen ions of CO_3^{2-} lie for the "perfect $3R_1$ crystal (polytype)" in register to neighboring OH^- ions of the octahedrons above and below, their centers are in register to Fe^{2+} ions, one above and

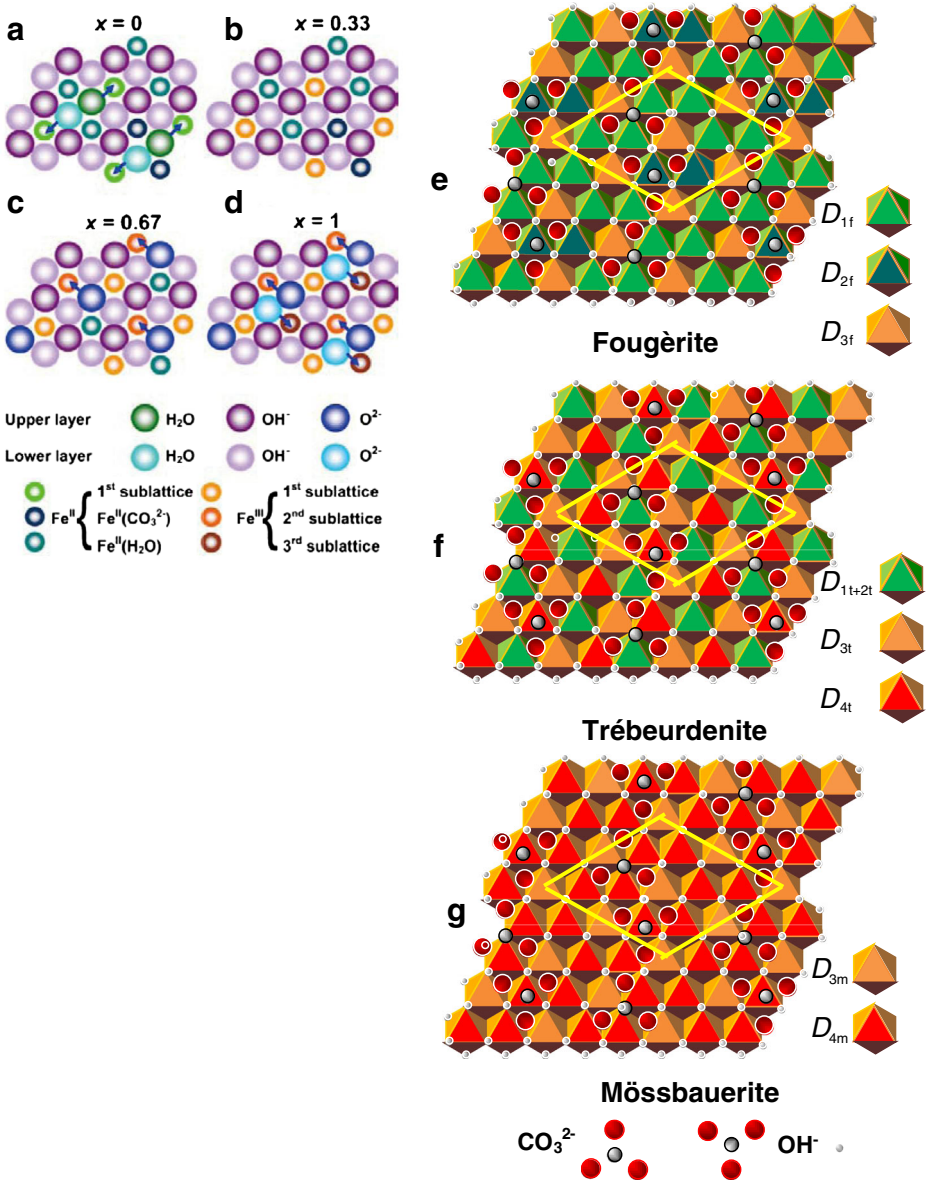

Fig. 10 Views of octahedral sites for various values of $x = \{[Fe^{III}]/[Fe_{total}]\}$ to distinguish the anions or molecules surrounding Fe cations. *Arrows* designate the cation to which must be attributed anions or molecules taking stoichiometric GR(CO_3^{2-}) as a reference. **a** Ferrous GR(CO_3^{2-})[§] at $x = 0$, some H_2O are replacing OH^- ions; **b** GR(CO_3^{2-}) at $x = (1/3)$, the first sublattice is filled with Fe^{III} ions and there exist only OH^- ions; **c** The second sublattice is filled with Fe^{III} ions and O^{2-} ions substitute OH^- ions in the upper layer; **d** Ferric GR(CO_3^{2-})* at $x = 1$, all cations are Fe^{III} and O^{2-} ions substitute OH^- ions in both lower and upper layers. **e–g** The octahedral site layers and one of the six interlayer configurations that lie above. Quadrupole doublets of the spectra correspond to sites as in the text

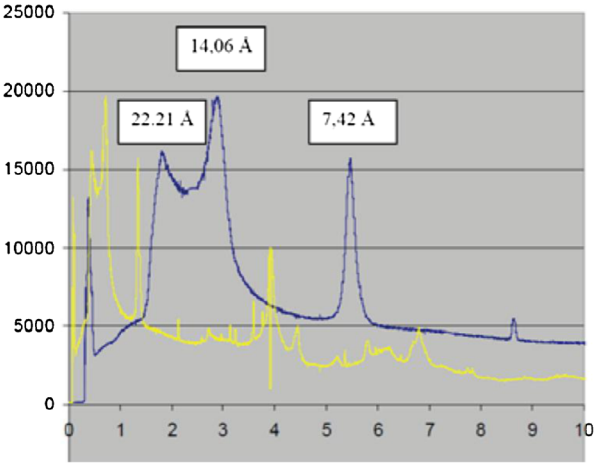

Fig. 11 Low angle diffraction peaks versus angle θ (in *yellow*) of a synthetic *mössbauerite* sample recorded with a 0.35 Å synchrotron radiation and its conversion into Mo Kα radiation ($\lambda = 0.7093$ Å) in *blue*. Three sets of peaks are seen around 22.21 Å, 14.06 Å and 7.42 Å; the first one originates from (001) peaks of the $3R_1$ and $3R_2$ polytypes, the second one from (001) peaks of the $2H_1$ and $2T$ polytypes and the third one from (003) peaks of the first polytypes

one below, explaining why 2 Fe^{2+} ions among 12 Fe cations contribute to the abundance of doublet D_2, i.e. 1/6 (Fig. 12).

The usual nomenclature $A\beta C{=}C\alpha B{=}B\gamma A{=}A\beta C$ used for the hydrotalcite supergroup [4] should be more adequately written here $A\beta C(=c=)C\alpha B(=b=)B\gamma A(=a=)A\beta C$ where a, b and c represent the positions of the oxygen of the CO_3^{2-} anions in the interlayers, since the 2D long range order within the CO_3^{2-} anion interlayer must be taken into account; $A(=a=)A$ means a "*P*-type" interlayer configuration as defined in [4]. This feature obtained in this very case from the Mössbauer data should probably be extended to other minerals of the hydrotalcite supergroup. These 2D long range orders for a cation sublayer as well as an anion interlayer corresponds to six possible orientations for the CO_3^{2-} ordering in interlayers for 120° rotations clockwise and anticlockwise. This was the state of the model already published [1, 12].

The model can be extended to other conceivable polytypes as reported in [4]. Each oxygen of CO_3^{2-} anion in the way between OH^- ions which are in register one to the other one lies in register to them, e.g. $B(=b=)B$. For a similar reason, in polytypes where exist offsets such as in $2T$ polytype, the stacking sequence becomes $A\beta C(-a-)B\gamma A(=a=)A\beta C$, i.e. it means that $C(-a-)B$ is the "*O*-type", counterpart of $A(=a=)A$. Each O^{2-} ions of CO_3^{2-} anions is the center of symmetry of adjacent OH^- ions. Thus, there exist: (i) the $3R_1$ polytype, $A\beta C(=c=)C\alpha B(=b=)B\gamma A(=a=)A\beta C$, which is the "perfect crystal", with a repeat along the $\boldsymbol{c}$ axis of ~22.21 Å giving (003) and (001) lines (Fig. 9), (ii) the $2H_1$ polytype, $A\beta C(=c=)C\beta A(=\mathrm{a}=)A\beta C$ that will correspond to a repeat of 14.78 Å, (iii) the $2T$ polytype, $A\beta C\text{-}a\text{-}B\gamma A(=a=)A\beta C(\text{-}a\text{-})B\gamma A$, with a repeat along $\boldsymbol{c}$ axis of 14.06 Å as observed in the x-ray pattern at low angles (Fig. 11) and (iv) $A\beta C(\text{-}a\text{-})B\gamma A(\text{-}b\text{-})C\alpha B(\text{-}c\text{-})A\beta C$, the $3R_2$ polytype, which corresponds to a repeat of 20 Å (Fig. 13). All these polytypes are consistent with both the XRD patterns and the Mössbauer spectra: Other polytypes gathered in the nomenclature at a time when ordering of CO_3^{2-} anions in interlayers was not yet admitted on the basis of sole XRD results are not eligible; they all correspond to a starting stacking sequence $A\beta C(\text{-}b\text{-})A\ldots$ It would mean that Fe cations of sublayer β are in register to O^{2-} ions of carbonate of interlayer (-*b*-) that lies just above it and such a configuration is contradictory to the Mössbauer observation.

The stacking sequences displayed for the four polytypes, i.e. $3R_1$, $2T$, $3R_2$ and $3H_1$ have ions at scale and the periodicity along the $\boldsymbol{c}$ axis for each polytype can be easily evaluated

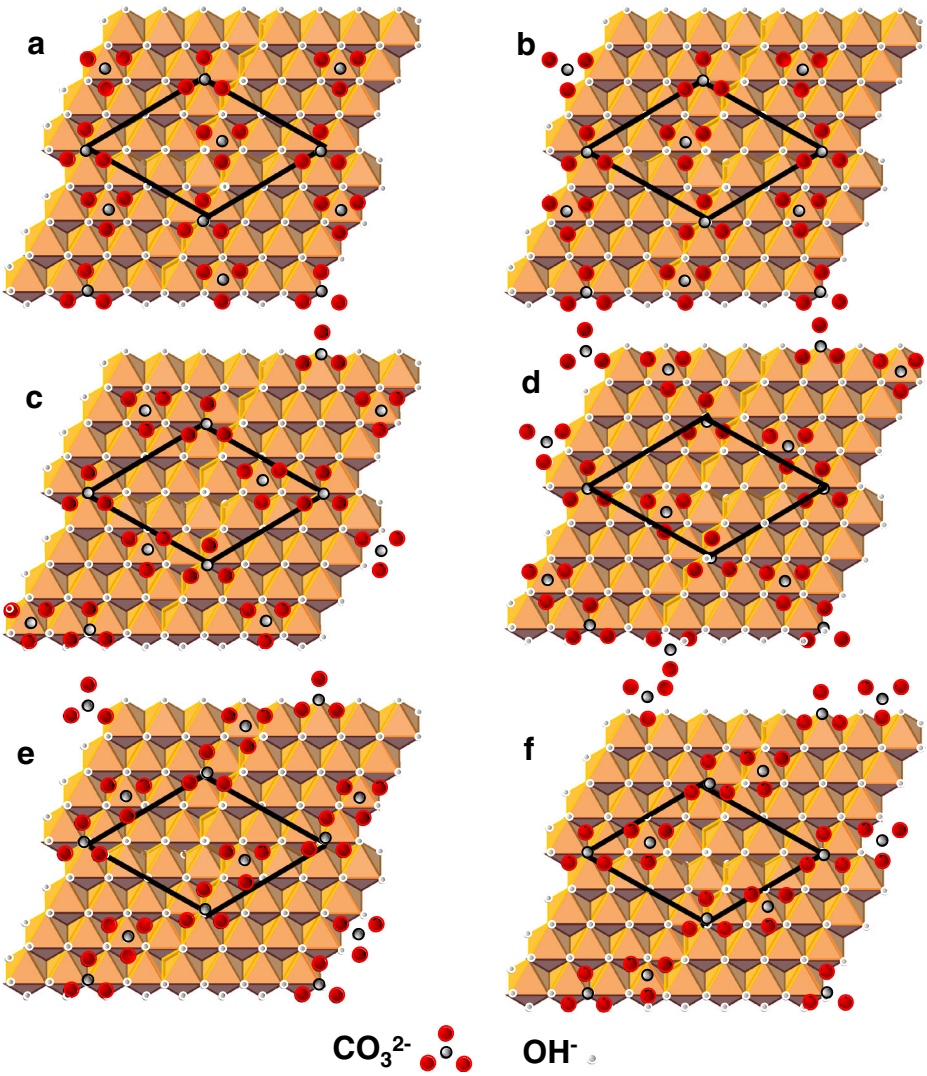

Fig. 12 The six possible configurations of a carbonate interlayer above a layer made of Fe^{3+} ions surrounded by OH^- and O^{2-} ions at the apices of the octahedral sites in e.g. *mössbauerite*. It is at the origin of the various polytypes that are revealed by the diffraction patterns; no coupling exists between anion interlayers inducing several stacking sequences

since in any stacking sequence e.g. in *A(-b-)C* or *AβC*, the OH^- sublayers *A* or *C* and "*O*-type" interlayer (*-b-*) have the same thickness X (Fig. 13); the size of OH^- anions is the same as that of the oxygen ions of CO_3^{2-} anions since it is not in the ***c*** axis direction, which the proton is pointing at. In contrast, a sequence of type *A(=a=)A* corresponds to a larger thickness Y for the "*P*-type" interlayer (=*a*=) since some room is needed for the two protons that point along the ***c*** direction. Experimentally, the (001) line of GR(CO_3^{2-}) corresponding to 22.21 Å and a strong line corresponding to 14.06 Å are observed at small angles (Fig. 11).

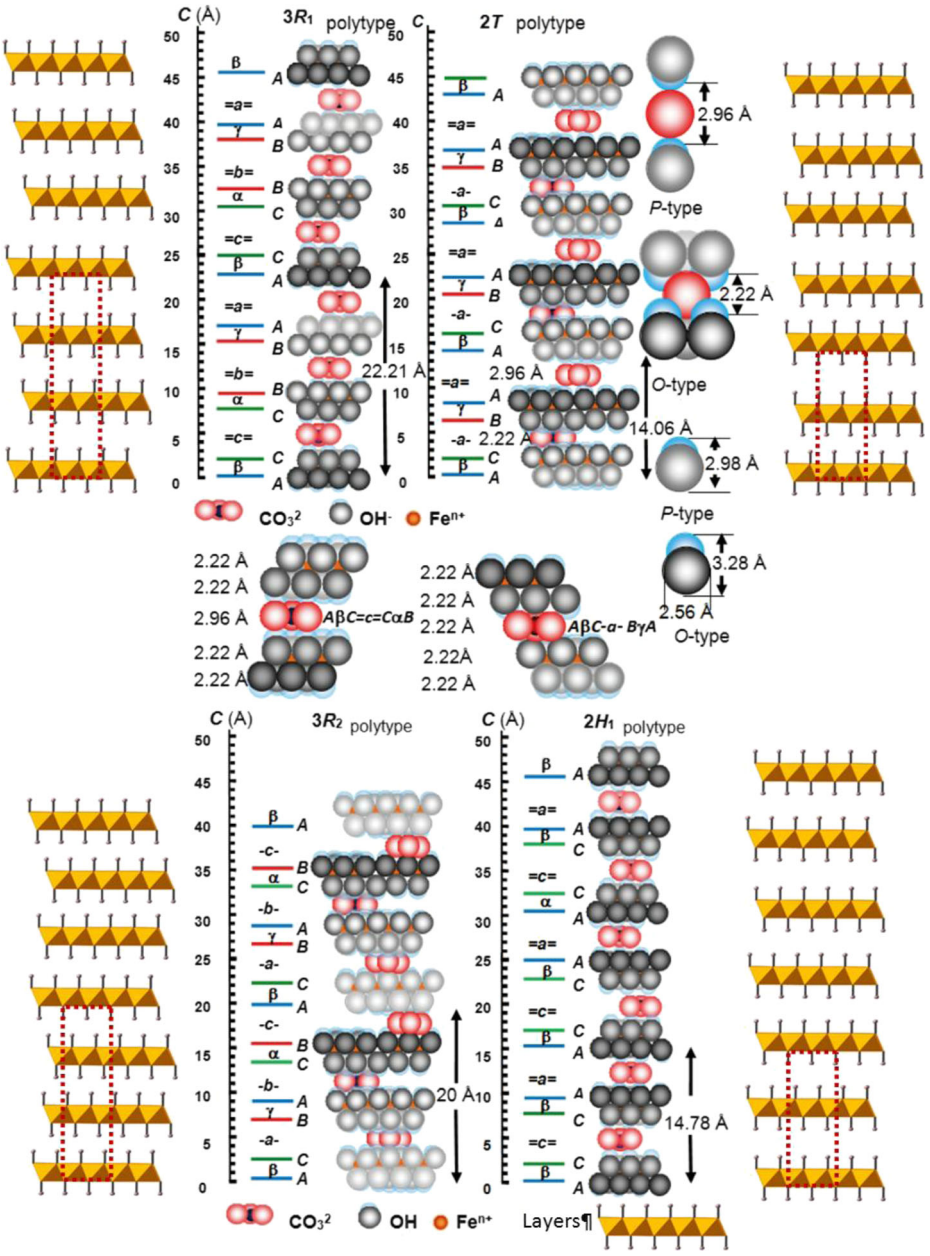

Fig. 13 View parallel to the ***c*** axis of the stacking of Fe^{n+} layers and CO_3^{2-} anions interlayers in the four polytypes found in the minerals of the "*fougèrite* group". OH^- and O^{2-} ions sublayers are displayed; ionic radii are respected. The thickness of each stratum was computed from the values of the repeat in polytypes $3R_1$ and $2T$ as observed by synchrotron radiation with a wavelength of 0.35 Å in *mössbauerite*

Relations are, (i) from $A\beta C(=c=)C\alpha B(=b=)B\gamma A(=a=)A\beta C$, i.e. $3R_1$ polytype, (6X + 3Y) = 22.21 Å and (ii) from $A\beta C(\text{-}a\text{-})B\gamma A(=a=)A\beta C$, i.e. $2T$ polytype, (5X + Y) = 14.06 Å. Thus, the thickness X attributed to each OH^- sublayer and "*O*-type" interlayer is worth ∼2.22 Å whereas the thickness Y attributed to each "*P*-type" interlayer is worth ∼2.96 Å. From the thickness X the radius R of O^{2-} ions is $R = X \times (2/\sqrt{3}) = 2.22 \times (2/\sqrt{3}) \sim 2.56$ Å. This occurs to be the most widely accepted value for the ionic radius of O^{2-} confirming the validity of the model; the O^{2-} ions belonging to CO_3^{2-} anions lie at the centre of symmetry of OH^- ions at the apices of the octahedrons, above and below, whatever the stacking sequence, either *A(-c-)B* or *A(=a=)A*. The spacing Y of 2.96 Å necessary for the interlayers in the *A(=a=)A* configuration comes from the protons in OH^- ions since the O^{2-} ions of CO_3^{2-} lie in register to these protons, which is not the case for *A(-c-)B* configuration that leads to a close packed stacking. Finally, the "thickness" of one OH^- ion pointing along the ***c*** axis in the "*O*-type" interlayer is 3.28 Å, the usual size, whereas in the "*P*-type" interlayer, where it is compressed, it is only 2.98 Å (Fig. 13). All these evaluations were recorded for the *mössbauerite* synthetic sample (Fig. 11). Finally, in the absence of experimental technique similar to Mössbauer spectroscopy, there is no sound reason why the same 2D ordering within cation layers and anion interlayers could not be extended to all other minerals belonging to the supergroup of hydrotalcite. However , this not yet proved experimentally.

5 The three minerals in gleys

5.1 Mössbauer spectroscopy

Mössbauer spectra were measured from natural gley samples and fitting used Lorentzian-shaped lines. The spectrum of a synthetic sample with $x = 1/2$ (Fig. 14a) was compared with that of a sample extracted from below the water table in the forest of Fougères (Fig. 14b); the spectra are nearly identical and only two quadrupole doublets are resolved in both cases. Four samples extracted from maritime marshes display spectra that were qualitatively quite different from those of Fig. 14a–b; the first one from Trébeurden was measured at room temperature (Fig. 14c) whereas the three others were from the Bay of Mont Saint-Michel (Fig. 14d–f) at 78 K. These spectra are qualitatively quite different from those of Fig. 14a–b. The spectrum from Trébeurden clearly resembles those from Saint Michel bay rather than that from Fougères, despite the higher temperature of experimental measurement. Spectral resolution was found to be somewhat poorer for natural samples than its synthetic counterpart, so a simpler method for fitting was employed, replacing the convolution of Gaussian distributions with Lorentzian-shaped lines by broadened Lorentzian-shaped lines . One Fe^{2+}doublet was sufficient since D_{1f}, D_{2f}, D_{1t} and D_{2t} could hardly be distinguished in the range [1/3-2/3]. In contrast, three doublets were necessary in the range [2/3-1]: one Fe^{2+} doublet ($D_{1t} + D_{2t}$), one Fe^{3+} doublet with a larger intensity that represents ($D_{3t} + D_{4t}$), and a third doublet that represents ($D_{3m} + D_{4m}$), with a larger quadrupole splitting and broader line-width. This simplified procedure gave excellent results for spectra measured at 78 K and Mössbauer parameters of Fig. 14c–f are given in Table 4.

The difference between spectra of Fig. 14b–f arises because gleys from below the water tables in Fougères have x in the [1/3-2/3] range, while those from salt marshes have $x > 2/3$. Marshes are covered by water only at high tide and the gley gets partially oxidized reaching a steady-state x value higher than for permanently waterlogged aquifers. Samples extracted from Trébeurden and the Bay of Mont Saint- Michel all have x values belonging to

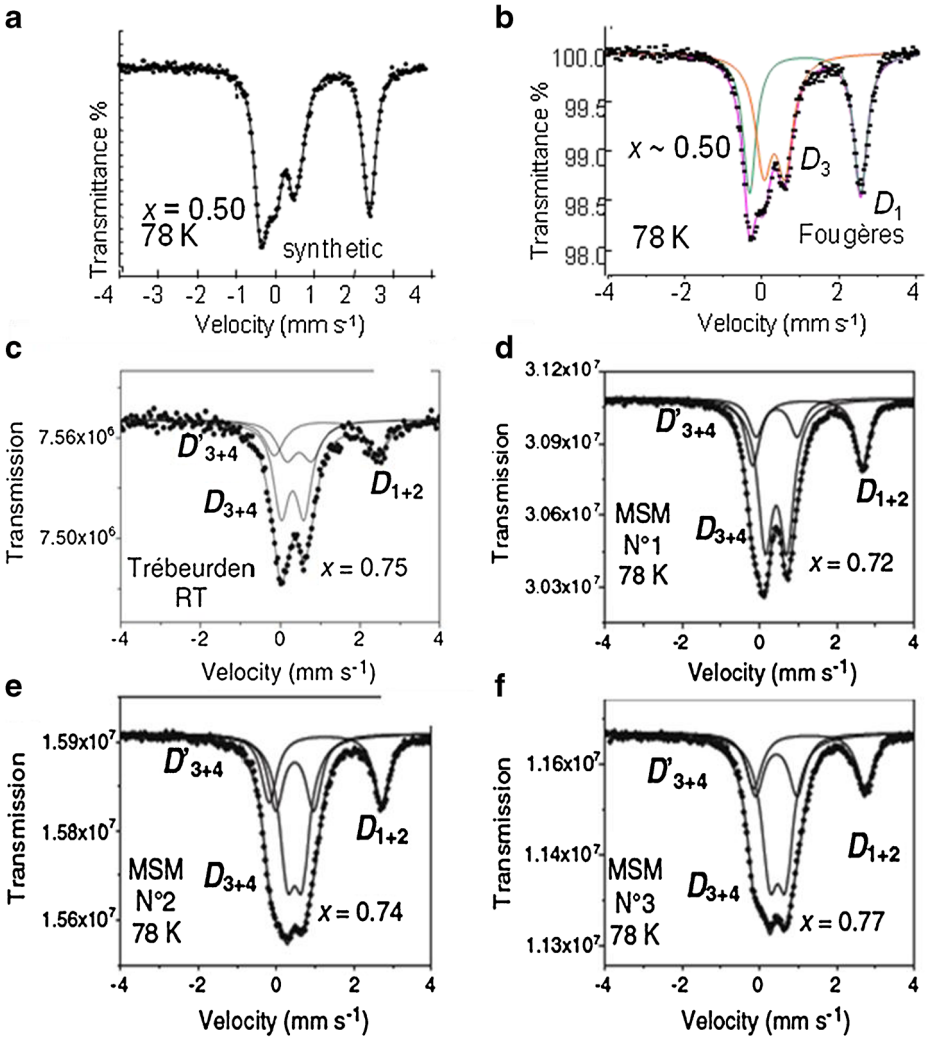

Fig. 14 Mössbauer spectra of samples extracted from maritime gleys: **a** Trébeurden measured at room temperature, **b–d** Mont-Saint-Michel bay measured at 78 K

[0.72–0.77] according to data of Table 4. The linear variation of intensities with composition is consistent with mechanical mixing of various proportions of *trébeurdenite* and *mössbauerite* (Fig. 15).

The partially resolved experimental doublet intensities into components that correspond to all the distinct Fe^{2+} and Fe^{3+} environments can be further decomposed

(i) Total $D_{3t} + D_{3m}$ is always 33.33%.
(ii) Intensities of D_{1f}: D_{2f} and D_{1t}: D_{2t} are always in a 3:1 ratio.
(iii) Intensity ratio D_{2f}: $D_{3f} = 1{:}4$; hence $(D_{1f} + D_{2f}) = D_{3f} = D_{4f}$.

Table 4 Mössbauer parameters for quadrupole doublets in gley samples extracted from maritime marshes

Quadrupole doublet		$D_{1t}+D_{2t}$ Fe^{2+}(T)	$D_{3t}+D_{4t}$ Fe^{3+}(T)	$D_{3m}+D_{4m}$ Fe^{3+}(M)
Trébeurden measured at room temperature				
	δ (mm s^{-1})	1.294	0.301	0.307
$x = 0.75$	Δ (mm s^{-1})	2.66	0.549	0.972
	RA (%)	25	50	25
	Γ (mm s^{-1})	0.56	0.45	0.49
Mont Saint-Michel Bay measured at 78 K				
N°1	δ (mm s^{-1})	1.245	0.429	0.441
$x = 0.72$	Δ (mm s^{-1})	2.842	0.560	1.059
	RA (%)	28	56	16
	Γ (mm s^{-1})	0.45	0.49	0.50
N°2	δ (mm s^{-1})	1.263	0.471	0.470
$x = 0.74$	Δ (mm s^{-1})	2.908	0.381	0.986
	RA (%)	26	52	22
	Γ (mm s^{-1})	0.45	0.49	0.50
N°3	δ (mm s^{-1})	1.292	0.466	0.434
$x = 0.77$	Δ (mm s^{-1})	2.877	0.405	1.073
	RA (%)	23	46	31
	Γ (mm s^{-1})	0.45	0.49	0.50

T*: trébeurdenite,* ***M****: mössbauerite*. δ: isomershift (reference is metallic iron at room temperature, Δ: quadrupole splitting, *RA*: relative abundance, Γ: line-width at half maximum

(iv) Intensity of D_{3m}: D_{4m} is always in a 1:2 ratio.

This partitioning for the spectra of maritime marshes (Table 4) is compared with the synthetic sample of the most similar composition (Fig. 4h and Table 2). The D_3 and D_4 peaks have been recombined according to the assignment schemes for both Tables 2 and 5; the expected relative areas for the synthetic sample are within 2% of those given in Table 2, demonstrating that the model, combined with the two doublet assignment schemes, applies to datasets from both the synthetic and natural samples, even though spectral fitting methods are different. Thus, the relative proportions for D_1–D_4 sites as a function of bulk composite can be drawn for $x \in$[1/3-1] (Fig. 15).

Since there are distinct variants of D_1 and D_2 for *fougèrite* and *trébeurdenite*, and three versions of D_3 for all minerals and two of $D_4$for *trébeurdenite* and *mössbauerite*, there are nine iron environments in the three minerals as a whole. Fe cation ordering allows us to deduce the identities of edge-sharing neighbour cations (Fig. 8); the Fe^{3+} ions of fougèrite, i.e. D_{3f}, are obviously situated above and below interlayer carbonate anions due to charge interaction. The constant proportion of D_3 in all three minerals confirms that this is maintained throughout the series, in which case the cation ordering can be deduced for the site types D_1–D_4. If the O^{2-} anions in the hydroxide sublayer, produced by deprotonation are required to be bonded to D_4 cations, the local environments around the Fe sites can be characterized (Table 6) with their distribution between minerals (Table 7).

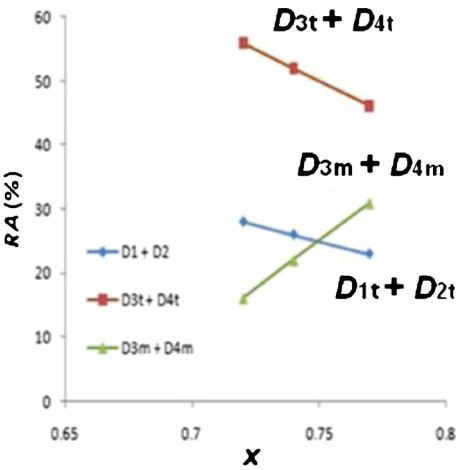

Fig. 15 Variation of relative areas for Mössbauer doublets $D_{1t}+D_{2t}$, $D_{3t}+D_{4t}$ and $D_{3m}+D_{4m}$ as a function of composition x for the data of Table 4

Table 5 Expected relative abundances of distinct Fe cation environments corresponding to Mössbauer spectra of Fig. 14c–f and Table 4, with the synthetic specimen at x = 0.78 (Fig. 14h) and Table 2 for comparison

	Trébeurden	Mont Saint Michel #1	Mont Saint Michel #2	Mont Saint Michel #3	Synthetic
x	0.75	0.72	0.74	0.77	0.78
T mol%	75	84	78	69	66
M mol%	25	16	22	31	34
D_{1t}%	18.75	21	19.5	17.25	16.5
D_{2t}%	6.25	7	6.5	5.75	5.5
D_{3t}%	25	28	26	23	22
D_{4t}%	25	28	26	23	22
D_{3m}%	8.33	5.33	7.33	10.33	11.33
D_{4m}%	16.67	10.67	14.67	20.67	22.67
$D_{3t}+D_{3m}$	33.33	33.33	33.33	33.33	33.33
$D_{4t}+D_{4m}$	33.33	38.67	40.67	43.67	44.67
$D_{3t}+D_{4t}$	50	56	52	46	44
$D_{3m}+D_{4m}$	25	16	22	31	34

Since intermediate compositions are intergrowths of phases with x = 1/3, 2/3or 1, any mineral sample in the range [1/3-2/3] is a mixture of *fougèrite* (***F***) and *trébeurdenite* (***T***), with proportions obtained by the lever rule $[(2\text{-}3x)\boldsymbol{F}+(3x\text{-}1)\boldsymbol{T}]$, whereas compositions in the [2/3-1] range are mixtures of ***T*** and *mössbauerite* (***M***) with the proportions $3(1\text{-}x)\boldsymbol{T}$ + $(3x\text{-}2)\boldsymbol{M}$. To date, occurrences of gleys extracted from continental aquifers as in Fougères only show compositions of $x \in$[1/3-2/3], while those from salt marsh environments such as in Trébeurden or Mont Saint-Michel Bay only show $x \in$[2/3-1].

Based on the data and analysis above, the International Mineralogical Association accepted:

(i) The former "*fougèrite*" named initially according to the forest of Fougères [14, 17] is redefined as the Fe^{II-III} hydroxycarbonate with formula $Fe_4^{2+}Fe_2^{3+}(OH)_{12}CO_3\cdot$

Table 6 Local environments for Fe cations

Local environment type	Cation	Edge-sharing octahedral neighbours	Interlayer species in vertical registry	Ligands in octahedral layer
D_{1f}	Fe^{2+}	3 Fe^{2+} + 3 Fe^{3+}	H_2O	$(OH)_6$
D_{2f}	Fe^{2+}	3 Fe^{2+} + 3 Fe^{3+}	CO_3^{2-}	$(OH)_6$
D_{3f}	Fe^{3+}	6 Fe^{2+}	CO_3^{2-}	$(OH)_6$
D_{1t}	Fe^{2+}	6 Fe^{3+}	H_2O	$(OH)_6$
D_{2t}	Fe^{2+}	6 Fe^{3+}	CO_3^{2-}	$(OH)_6$
D_{3t}	Fe^{3+}	3 Fe^{2+} + 3 Fe^{3+}	CO_3^{2-}	$(OH)_{5.33}O_{0.67}$
D_{4t}	Fe^{3+}	3 Fe^{2+} + 3 Fe^{3+}	H_2O	$(OH)_4O_2$
D_{3m}	Fe^{3+}	6 Fe^{3+}	CO_3^{2-}	$(OH)_4O_2$
D_{4m}	Fe^{3+}	6 Fe^{3+}	H_2O	$(OH)_4O_2$

Table 7 Abundances of local Fe environments in the "*fougèrite* group" minerals

	D_1		D_2		D_3			D_4	
	D_{1f}	D_{1t}	D_{2f}	D_{2t}	D_{3f}	D_{3t}	D_{3m}	D_{4t}	D_{4m}
Fougèrite	50%		16.7%		33.3%				
Trébeurdenite		25%		8.3%		33.3%		33.3%	
Mössbauerite							33.3%		66.7%

$3H_2O$, at $x = 1/3$; it is the common $Fe^{II–III}$LDH, often called "carbonated green rust" that is observed during the corrosion of Fe-based materials and steels (e.g. [6]).

(ii) The $Fe^{II–III}$ oxyhydroxycarbonate at $x = 2/3$ with formula $Fe_2^{2+}Fe_4^{3+}O_2(OH)_{10}CO_3 \cdot 3H_2O$ as *trébeurdenite*, named for the township, Trébeurden, near the maritime marsh where the mineral was first found. The holotype specimen M52133 is housed in the collections of Museum Victoria in Melbourne (Australia) from the type locality Penvern that faces Île d'Aval in Trébeurden, Brittany, France.

(iii) The ferric oxyhydroxycarbonate with $x = 1$ and formula $Fe_6^{3+}O_4(OH)_8CO_3 \cdot 3H_2O$ is named *mössbauerite*, after Professor Rudolf Mössbauer (1928–2011) who discovered the resonance of γ rays that bears his name, and for which he was awarded the 1961 Nobel Prize in physics. A full type description of *mössbauerite* will be soon reported.

5.2 XRD

A direct analysis of natural *mössbauerite* is not yet possible since it is intergrown with the closely related mineral *trébeurdenite* as well as having nanometre sized grains. Separation of the combined "green rust" minerals from other phases in the gley was not even possible, given their small modal abundance, small grain size and rapid decomposition when exposed to air. Detection and characterisation of *mössbauerite* relies on techniques that can

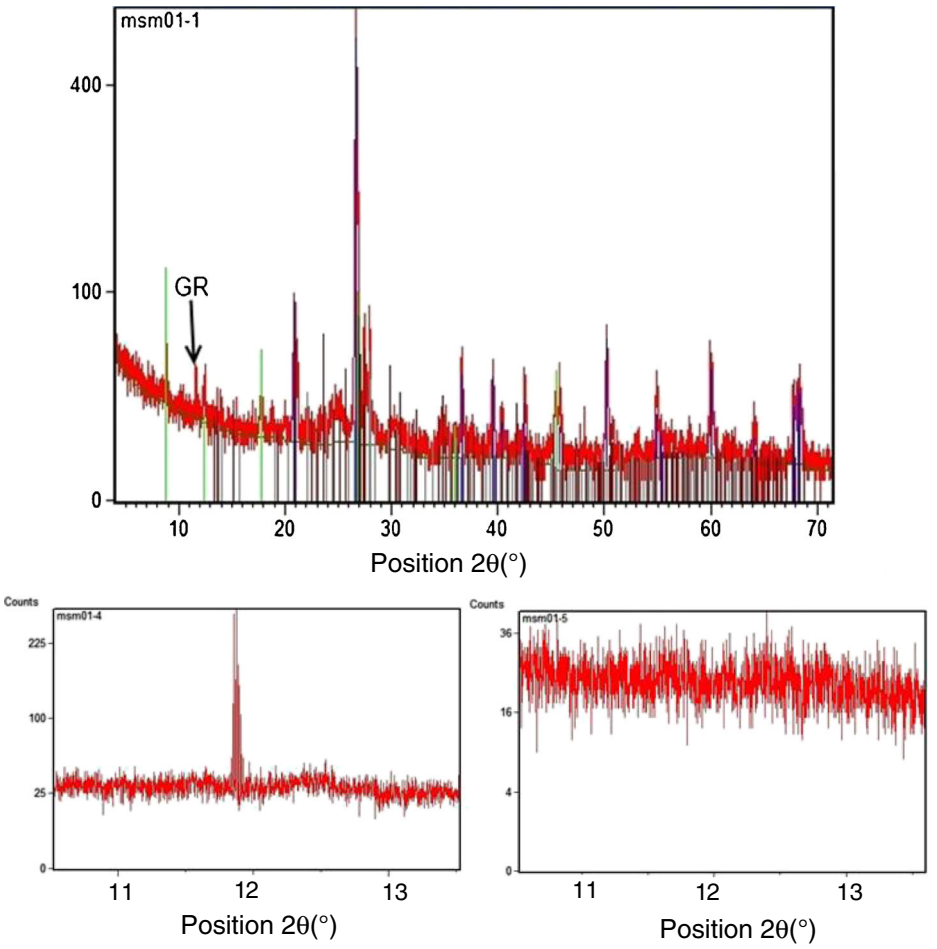

Fig. 16 *Top*: PXRD diagram of wet gley from Mont Saint-Michel Bay. Note the *green rust* peak which is not matched by other phases in the gley. GR = "*trébeurdenite* + *mössbauerite*, i.e. "*green rust*". *Green lines* are illite, *blue* are quartz, *brown* are orthoclase and *grey* are albite. *Bottom*: "*Green rust*" (*trébeurdenite* + *mössbauerite*). d_{003}peak in wet gley (*left*) and the same gley mount which had dried after several hours (*right*) showing no "*green rust*". Sample from Mont Saint-Michel Bay. $d_{003} = 7.449$ Å

be applied to multiphase samples with minimal sample preparation, in particular, the eponymous spectroscopic method, and comparison with synthetic standard materials. The type material, while wet with an excess of its associated seawater, gave an XRD peak corresponding to d_{003} of *mössbauerite* + *trébeurdenite* at an intensity implying a few percent by mass of the total sample (Fig. 16a-b). It is for only the d_{003} line of the "*fougèrite* group" minerals to be distinguishable in X-ray diffraction (XRD) patterns of natural material; other lines overlap with those of the common minerals found in gleys. In some cases, the d_{006} may also be observed. This Mössbauer study proved coexistence of the two "green rust" minerals, *trébeurdenite* and *mössbauerite*, (Fig. 14). After drying the sample, the diagnostic XRD peak disappeared due to decomposition of the phases (Fig. 16c), which presumably lost CO_2 and H_2O and oxidized to form a poorly crystalline Fe oxyhydroxide such as ferrihydrite. This decomposition path was also shown to exist in synthetic samples (e.g. [6, 10]).

6 Conclusion

This complete survey about the structure and some occurrences of ≪ green rust ≫ related new minerals of the ≪ *fougèrite* group≫, *trébeurdenite* and *mössbauerite*, belonging to the ≪ hydrotalcite supergroup≫ [4] demonstrates the valuable information complementary to XRD obtained from Mössbauer spectroscopy. In particular, it shows that a 2D long range order exists among Fe^{3+} ions in the cation hexagonal pavements and correlatively a 2D long range order among CO_3^{2-} anions in interlayers. During the oxidation process by *in situ* deprotonation starting from *fougèrite* to *trébeurdenite* and finally *mössbauerite*, the 2D order of anions in interlayers stays unchanged as proved from Mössbauer data. Consequently, the absence of superlattice lines in XRD patterns can only be explained by the presence of various polytypes destroying the periodicity along the ***c*** axis of the LDH, the existence of which was fully discussed with the small angle diffraction experiment performed at the Zürich synchrotron. A question arises: why should it be different for the other minerals of the "hydrotalcite supergroup"?

Acknowledgments Special thanks are devoted to Pr. A. Herbillon from the University of Louvain la Neuve (Belgium) and Dr. O. Guérin of Ecole Pratique des Hautes Etudes-Paris Sorbonne who provided the maritime marsh samples. Pr. Michel François (Université de Lorraine) rand the synchrotron experiment.

References

1. Génin, J.-M.R., Ruby, C., Upadhyay, C.: Structure and thermodynamics of ferrous, stoichiometric and ferric oxyhydroxycarbonate green rusts; redox flexibility and fougèrite mineral. Solid State Sci. **8**, 1330–1343 (2006)
2. Ruby, C., Upadhyay, C., Géhin, A., Ona-Nguema, G., Génin, J.-M.R.: In situ redox flexibility of Fe^{II-III} oxyhydroxycarbonate green rust and fougèrite. Environ. Sci. Technol. **40**, 4696–4702 (2006)
3. Génin, J.-M.R., Renard, A., Ruby, C.: Fougèrite Fe^{II-III} oxhydroxycarbonate in environmental chemistry and nitrate reduction. Hyperfine Interact. **186**, 31–37 (2008)
4. Mills, S.J., Christy, A.G., Génin, J.-M.R., Kameda, T., Colombo, F.: Nomenclature of the hydrotalcite supergroup: natural layered double hydroxides. Mineral. Mag. **76**, 1289–1336 (2012)
5. Génin, J.-M.R., Olowe, A.A., Refait, Ph., Simon, L.: On the stoichiometry and Pourbaix diagram of Fe(II)-Fe(III) hydroxysulphate or sulphate-containing green rust 2: An electrochemical and Mössbauer spectroscopy study. Corros. Sci. **38**, 1751–1762 (1996)
6. Drissi, S.H., Refait, Ph., Abdelmoula, M., Génin, J.-M.R.: The preparation and thermodynamic properties of Fe(II)-Fe(III) hydroxycarbonate (green rust 1); Pourbaix diagram of iron in carbonate-containing aqueous media. Corros. Sci. **37**, 2025–2041 (1995)
7. Gancedo, J.R., Martínez, M.L., Oton, J.: Mössbauer spectroscopy study of corrosion products of iron with ammonium nitrate in aqueous solutions. J. Phys. **37**(C6), 297–299 (1976)
8. Bernal, J.D., Dasgupta, D.R., Mackay, A.L.: The oxides and hydroxides of iron and their structural inter-relationships. Clay Miner. Bull. **4**, 15–30 (1959)
9. Génin, J.-M.R., Abdelmoula, M., Ruby, C., Upadhyay, C.: Speciation of iron; characterization and structure of green rusts and Fe^{II-III} oxyhydroxycarbonate fougerite. Compt. R. Geosci. **338**, 402–418 (2006)
10. Benali, O., Abdelmoula, M., Refait, Ph., Génin, J.-M.R.: Effect of orthophosphate on the oxidation products of Fe(II)-Fe(III) hydroxycarbonate: the transformation of green rust to ferrihydrite. Geochim. Cosmochim. Acta **65**, 1715–1726 (2001)
11. Génin, J.-M.R., Ruby, C., Géhin, A., Refait, Ph.: Synthesis of green rusts by oxidation of $Fe(OH)_2$; their products of oxidation and reduction of ferric oxyhydroxides; E_h-pH Pourbais diagrams. Compt. R. Geosci. **338**, 433–446 (2006)
12. Génin, J.-M.R., Aïssa, R., Géhin, A., Abdelmoula, M., Benali, O., Ernstsen, V., Ona-Nguema, G., Upadhyay, C., Ruby, C.: Fougèrite and Fe^{II-III} hydroxycarbonate green rust: ordering, deprotonation and/or cation substitution; structure of hydrotalcite-like compounds and mythosic ferrosic hydroxide $Fe(OH)_{(2+x)}$. Solid State Sci. **7**, 545–572 (2005)

13. Legrand, L., Abdelmoula, M., Géhin, A., Chaussé, A., Génin, J.-M.R.: Electrochemical formation of a new Fe(II)-Fe(III) hydroxycarbonate green rust: characterisation and morphology. Electrochim. Acta **46**, 1815–1822 (2001)
14. Trolard, F., Abdelmoula, M., Bourrié, G., Humbert, B., Génin, J.-M.R.: Evidence of the occurrence of a 'green rusts' component in hydromorphic soils. Proposed existence of a new mineral fougerite. Comptes Rendus Acad. Sci. **323**(serie IIa), 1015–1022 (1996)
15. Trolard, F., Génin, J.-M.R., Abdelmoula, M., Bourrié, G., Humbert, B., Herbillon, A.J.: Identification of a green rust mineral in a reductomorphic soil by Mössbauer and Raman spectroscopies. Geochim. Cosmochim. Acta **61**, 1107–1111 (1997)
16. Génin, J.-M.R., Bourrié, G., Trolard, F., Abdelmoula, M., Jaffrezic, A., Refait, Ph., Maòtre, V., Humberts, B., Herbillon, A.J.: Thermodynamic equilibrium in aqueous suspensions of synthetic and natural Fe^{II}-Fe^{III} green rusts: occurrences of the mineral in hydromorphic soils. Environ. Sci. Technol. **32**, 1058–1068 (1998)
17. Génin, J.-M.R., Guérin, O., Herbillon, A.J., Kuzman, E., Mills, S.J., Morin, G., Ona-Nguema, G., Ruby, C., Upadhyay, C.: Redox topotactic reactions in $Fe^{II–III}$ (oxy)hydroxycarbonate new minerals related to fougerite in gleysols; "trébeurdenite" and "mössbauerite". Hyperfine Interact. **204**, 71–81 (2012)
18. Génin, J.-M.R., Bauer, Ph., Olowe, A.A., Rézel, D.: Mössbauer study of the kinetics of simulated corrosion process of iron in chlorinated aqueous solution around room temperature: the hyperfine structure of ferrous hydroxides and green rust I. Hyperfine Interact. **29**, 1355–1360 (1986)
19. Génin, J.-M.R., Refait, Ph., Simon, L., Drissi, S.H.: Preparation and E_h-pH diagrams of Fe(II)-Fe(III) green rust compounds; hyperfine interaction characteristics and stoichiometry of hydroxy-chloride, -sulphate and -carbonate. Hyperfine Interact. **111**, 313–318 (1998)
20. Géhin, A., Ruby, C., Abdelmoula, M., Benali, O., Ghanbaja, J., Refait, Ph., Génin, J.-M.R.: Synthesis of Fe(II-III) hydroxysulphate green rust by coprecipitation. Solid State Sci. **4**, 61–66 (2002)
21. Refait, Ph., Charton, A., Génin, J.-M.R.: Identification, composition thermodynamic and structural properties of a pyroaurite-like Fe(II)-Fe(III) hydroxy-oxalate green rust. Eur. J. Solid State Inorg. Chem. **35**, 655–666 (1998)
22. Génin, J.-M.R., Simon, L., Refait, Ph.: Existence of sulphide-containing green rust one. Il nuovo cimento **50**, 55–58 (1996)
23. Génin, J.-M.R., Ruby, C.: Composition and anion ordering in some $Fe^{II–III}$ hydroxysalt green rusts (carbonate, oxalate, methanoate); the fougèrite mineral. Solid State Sci. **10**, 244–259 (2008)
24. Ruby, C., Abdelmoula, M., Naille, S., Renard, A., Khare, V., Ona-Nguema, G., Morin, G., Génin, J.-M.R.: Oxidation modes and thermodynamics of $Fe^{II–III}$ oxyhydroxycarbonate green rust: dissolution-precipitation versus in situ deprotonation. Geochim. Cosmochim. Acta **74**, 953–966 (2010)
25. Rusch, B., Génin, J.-M.R., Ruby, C., Abdelmoula, M., Bonville, P.: Mössbauer study of magnetism in FeII-FeIII (oxy)hydroxycarbonate green rusts; ferrimagnetism of Fe^{II}-Fe^{III} hydroxycarbonate. Hyperfine Interact. **187**, 7–12 (2008)
26. Rusch, B., Génin, J.-M.R., Ruby, C., Abdelmoula, M., Bonville, P.: Ferrimagnetic properties in Fe^{II}-Fe^{III} (oxy)hydroxycarbonate green rusts. Solid State Sci. **10**, 40–49 (2008)